IOP Publishing Nanotechnology
Nanotechnology 27 (2016) 485602 (11pp) doi:10.1088/0957-4484/27/48/485602

Engineering chemically exfoliated dispersions of two-dimensional graphite and molybdenum disulphide for ink-jet printing

Monica Michel[1], Jay A Desai[1], Chandan Biswas[2] and Anupama B Kaul[2,3]

[1] Metallurgical, Materials and Biomedical Engineering, University of Texas at El Paso, El Paso, TX 79968, USA
[2] Electrical and Computer Engineering, University of Texas at El Paso, El Paso, TX 79968, USA

E-mail: akaul@utep.edu

Received 13 May 2016, revised 29 September 2016
Accepted for publication 10 October 2016
Published 2 November 2016

Abstract

Stable ink dispersions of two-dimensional-layered-materials (2DLMs) MoS_2 and graphite are successfully obtained in organic solvents exhibiting a wide range of polarities and surface energies. The role of sonication time, ink viscosity and surface tension is explored in the context of dispersion stability using these solvents, which include N-methyl-2-pyrrolidone (NMP), *N*,*N*-Dimethylacetamide (DMA), dimethylformamide (DMF), Cyclohexanone (C), as well as less-toxic and more environmentally friendly Isopropanol (IPA) and Terpineol (T). The ink viscosity is engineered through the addition of Ethyl-Cellulose (EC) which has been shown to optimize the jettability of the dispersions. In contrast to prior work, the addition of EC *after* sonication—instead of *prior* to it—is noted to be effective in generating a high-density dispersion, yielding a uniform film morphology. High-quality inks are obtained using C/T and NMP as solvents for MoS_2 and graphite, respectively, as gauged through optical absorption spectroscopy. Electronic transport data on the solution-cast inks is gathered at room temperature. Arrays of 2D graphite-rod based inks are printed on rigid Si, as well as flexible and transparent polyethylene terephthalate (PET) substrates. The results clearly show the promise of ink-jet printing for casting 2DLMs into hierarchically assembled structures over a range of substrates for flexible and printed-electronics applications.

Keywords: 2D materials, inkjet printing, dispersion, molybdenum disulfide, graphene

(Some figures may appear in colour only in the online journal)

1. Introduction

The scotch tape-assisted exfoliation of graphene in 2004 [1] from parent graphite was a pivotal step in enabling the exploration of a wide range of graphene-like two-dimensional layered materials (2DLMs) [2]. There are a number of 2DLMs [3], ranging from: h-BN [4], transition metal dichalcogenides (e.g. MoS_2, $MoSe_2$ and WSe_2) [5], metal halides (e.g. PbI_2 and $MgBr_2$) [6], and tertiary compounds of carbo-nitrides [7]. These materials exhibit a weak inter-layer bonding through the van der Waals interaction, and thus have the potential to be mechanically exfoliated into nanosheets. Although mechanical exfoliation is a quick and effective means to produce individual, high-quality 2D nanosheets for fundamental investigation, this technique limits production to micron-sized fragments and is not amenable to scalability. Given that the layers are bonded through the weak van der Waals interaction, another possible avenue for isolating the 2D nanosheets is to chemically exfoliate the bulk crystals in liquids that yield higher density dispersions, which also offer prospects for large-area scalability [8]. Once the solution dispersions are formed, they can then be cast onto substrates using techniques such spray coating, doctor blading and gravure printing.

[3] Author to whom any correspondence should be addressed.

Another viable approach for dispersing the solutions onto a wide variety of substrates is through ink-jet printing which is a versatile technique for the large-area fabrication of flexible electronics [9, 10], requiring minimal process steps, and serves as one of the cornerstone processes for additive manufacturing [11]. Ink-jet printing has emerged as the approach for the rapid manufacturing of thin-film transistors (TFTs), which are constructed using organic conducting and semiconducting inks [12]. However, despite notable advances, ink-jet printed organic TFTs still show poor air stability, limited lifetime, low mobilities ($<0.5\ cm^2\ V^{-1}\ s^{-1}$) and the ON/OFF ratios are typically $<10^5$ [13]. Such limitations arise primarily from the poor quality of the materials used as the inks in such organic systems. In this paper, we report on forming 2DLM-based dispersions suitable for ink-jet printing, where the 2DLMs offer unique attributes, such as greater air-stability, higher-mobilities, and ease of chemical exfoliation given their unique crystal structures. While there are a wide variety of van der Waals solids, here we investigate the dispersion characteristics of two specific 2DLMs, i.e. metallic graphite and semiconducting MoS_2.

Prior to forming inks of these materials, the 2DLMs must first be dispersed as nanosheets in a liquid. Early work on solution-based exfoliation of graphite comprised of intercalated graphite which could be partially exfoliated by reactions involving an intercalant [14], through thermal shock [15], or by the shear oxidation of graphite [16]. The oxidation of graphite to yield graphene has resulted in fragments of oxidized sheets that exhibit significant structural defects and are often electrically insulating [17]. In this work, we have utilized ultrasonication, where cavitation bubbles generated using ultrasonic waves in a solvent, collapse into high-energy jets, and break up the layered crystallites into exfoliated nanosheets [18].

The choice of solvents used for exfoliation plays a key role for successfully isolating high-quality single layers of 2DLMs that are stable against re-aggregation. Modeling has shown that if the surface energy of the solvent is similar to that of the LM, the energy difference between the exfoliated and re-aggregated states will be very small, removing the driving force for re-aggregation [8]. Research shows that several organic solvents have cohesive energies close to the interlayer energies of 2DLMs, in particular the transition metal dichalcogenides, where the lattice can expand by as much as 100 times when they are dispersed in such solvents [19]. Through these deductions, the most promising solvents for achieving stable suspensions of 2DLMs appear to be N-methyl-2-pyrrolidone (NMP), *N*,*N*-Dimethylacetamide (DMA) and Dimethylformamide (DMF) [20–22], while hydrazine, cyclohexyl-pyrrolidinone (CHP), G-Butyrolactone (GBL), 1,3-Dimethyl-2-Imidazolidinone (DMEU) are also known to be effective. In this work we have explored the role of the first three solvents in forming suspensions of 2D MoS_2 and graphite, while also exploring the effect of less toxic and more environmentally friendly solvents such Isopropanol (IPA) and Terpineol (T).

For ink-jet printing, the ability to generate droplets, positioning the droplets onto specific locations on a substrate, the substrate-droplet interaction, and drying the solvents to yield a solid deposit, are key factors that determine the viability of the solution dispersions for ink-jet printing [23]. The most important physical parameters to consider for printing fluids are viscosity η, density ρ, and surface tension γ [23–25]. Here we have determined a way in which to utilize Ethyl Cellulose (EC), a cellulose in which some of the hydroxyl groups of the linear chain have been converted into ethyl groups, in order to engineer η of the dispersions; we have also measured its impact on γ of the fluid. In prior work, while EC has been shown to act as a stabilizing polymer and surfactant to prevent nanoparticle agglomeration [26, 27], here we note that it is more effective to incorporate EC *after* the sonication process instead of *prior* to it. To characterize the effectiveness of our dispersions, we have also relied upon optical absorption spectroscopy, which has long been used to quantify nanoparticle concentration through the use of the Lambert-Beer law [21, 28]. After forming stable dispersions, we proceeded to print test structures from the formulated inks and characterize their materials properties. In general, the ink-jet printed 2D nanosheets hold promise to enable the integration of a diverse array of 2DLMs in a single manufacturable platform, for the realization of hierarchically assembled vertical heterostructures on flexible, transparent or stretchable substrates, where 2DLMs have the potential to compete with traditional printed and organic electronics technologies.

2. Results and discussion

The quality of the inks used in ink-jet printing is mostly determined by forming a stable solute suspension, and controlling the solution η, ρ, and γ [29, 30]. Stable suspension of nanoparticles in a solvent are mainly dominated by Hansen solubility parameters (HPs) [31, 32], which contain (i) dipolar intermolecular forces, (ii) dispersion forces, and (iii) hydrogen bonding forces between the molecules [33, 34]. The dipolar interaction can be mostly controlled by the polarity P_i of the solvents [35, 36], and the dispersion forces require balancing the solvent-solvent, solvent-solute, and solute-solute binding energies. The hydrogen bonds increase the intermolecular attraction and they are known to outweigh the weaker van der Waals force. In this work, we have analyzed five solvents (see figure 1(a)) with differing P_i for 2DLM dispersions. The solvents studied were: (i) NMP ($P_i = 6.7$), (ii) DMA ($P_i = 6.5$), (iii) DMF ($P_i = 6.4$), (iv) Cyclohexanone (C)/T ($P_i = 4.5$), and (v) IPA ($P_i = 3.9$). Moreover, solvents with high P_i values (>6.4) such as NMP, DMA, DMF were investigated, while at the same time solvents with lower $P_i$values, such as C/T and IPA, were also explored.

In section 2.1 we discuss the importance of characterizing the viscosity and surface energy of the fluids, followed in section 2.2, where optical absorption spectroscopy is used to characterize the dispersion stability of MoS_2. In section 2.3, our analysis of graphite dispersions is discussed in the context of two different graphite starting templates, a graphite rod and commercially available graphite powder, while in section 2.4, the role of EC is elucidated in the context of particle

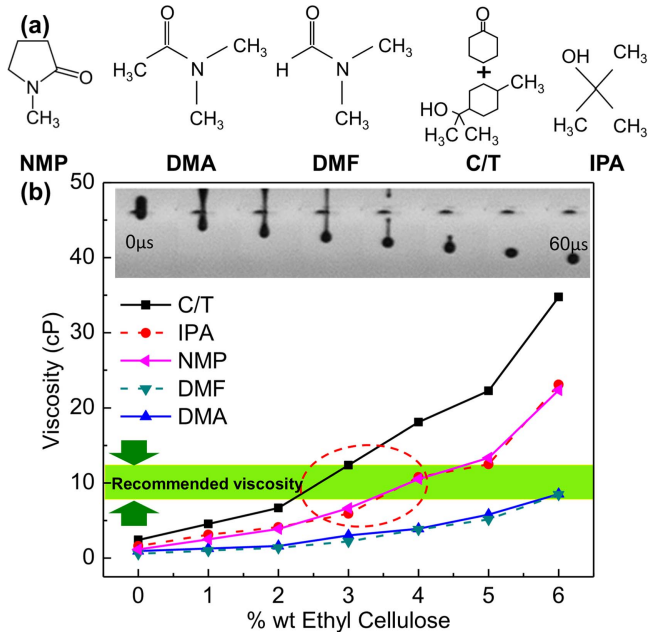

Figure 1. (a) Structural formulas of the five solvents studied in this work. (b) Graph showing the change in viscosity of the five solvents with the addition of EC and area of recommended viscosity values for inkjet printing. Inset shows successful drop formation and ejection from the printer nozzle with minimal satellite droplets.

dispersion optimization. Finally, in section 2.5 we delve into the electronic transport characteristics of the graphite dispersions, and comment on our ability to print arrays of these inks on several substrates in section 2.6.

2.1. Fluid viscosity and surface energy

A key property of inks that makes them viable for printing is the ability to generate droplets [23], which is intimately dependent on the ink η, γ, ρ, and nozzle diameter a. The printing procedure is likely to be sensitive to both the lateral flake size and the dispersion concentration. Once ejected, the drop behavior is also influenced by the choice of the substrate, where the droplet contact angle θ_c [37] is directly related to the substrate-ink surface energies; a large θ_c will cause the ink to de-wet the substrate, whereas a small θ_c will lead to poorly controlled features of the printed lines. In addition, the distance between the substrate and the ink-jet head must be optimized to guarantee both homogeneous printing and the highest resolution. A substrate very close to the nozzle will lead to secondary drops to scatter off during the impact of the primary drop, due to the initial drop-jetting pressure, which will affect the homogeneity of the final printed features [38]. A parameter that is often used to predict the jettability of a fluid is the so-called Ohnesorge number $Oh = \eta/\sqrt{\gamma\rho a}$ [25]. In most situations, ρ and a, are constant for a given fluid and printer settings, suggesting that Oh is intimately dependent on η and γ. In this work we have studied five solvents with different surface tensions ranging from 23 to 41 mJm^{-2}, polarities from 3.9 to 6.7, different functional groups, and molecular weights. The η and solvent polarity play an important role for determining optimum ink droplet formation and printability. Previous investigations demonstrate that the use of EC into the nanoparticle dispersion improves ink stability, pattern uniformity and does not leave significant residue after annealing [9, 26, 31]. In this work, we have shown that η and θ_c can be engineered through the addition of EC in all of the five solvents, to yield η in the range of 8–12 cP, which is in the regime appropriate for ink-jet printing (5–15 cP), as shown by the shaded region in figure 1(b). Here it should also be apparent that C/T showed the greatest increase in η, up to 15 times in going from 2.4 cP to 35 cP with the addition of 6 wt% EC. Therefore, C/T shows the optimum viscosity for ink-jet printing with the lowest EC concentration (~2.5 wt%) compared to all the other solvents. In comparison, at least 6 wt% EC needs to be added to bring DMA and DMF ink into the printing region (10 cP). The inset in figure 1(b) shows the obtained ink droplet for graphite nanoparticles in NMP with 4 wt% EC, demonstrating the drop dynamics of the prepared ink with minimal satellite droplets.

The addition of EC also affects the droplet θ_c on the substrate due to the change in η. Contact angle measurements were conducted using a goniometer with EC in the range of 1 to 6 wt%. Figure 2(a) illustrates the droplet shape just before it lands on the SiO_2 substrate, with drop diameter ~200 μm for C/T at 4 wt% EC (figure 2(b)), with θ_c shown in figure 2(c). Figure 2(d) indicates that θ_c increases for all five solvents with increasing EC concentration. The increase in θ_c of the solvent is likely to be due to the reduction of liquid surface tension with increasing EC concentration. It was evident from our investigation (figure 2(d)) that the increase in θ_c with increasing EC concentration was much higher for IPA which has the lowest P_i, as compared to C/T with the next lower P_i; it was almost identical for NMP, DMA, and DMF which have similar P_i. IPA and terpineol have hydroxyl groups (as can be seen in figure 1(a)) that form intermolecular hydrogen bonds, which as was mentioned above, is one of the parameters to consider for stable dispersions. These hydrogen bonds cause the molecules to 'stick' together and act as if they had a higher molecular weight. DMF and DMA have very similar structures and P_i values, with their only distinct feature being the hydrogen bond in DMF that is replaced with a methyl group in the DMA; this may result in a difference in the exfoliation, but almost no difference in their viscosity behavior is observed. From the data shown in figure 2(d), we see that there is an insignificant change in contact angle with the addition of EC for solvent NMP, which is also the same behavior noted for DMF and DMA. This is in contrast to IPA and C/T where the contact angle changed more significantly as more EC was added. Furthermore, the jetting properties and drop formation required for printing depend on both viscosity and surface energy. Since one of the main motivations of this work was to explore the use of EC as a viscosity modifier, and we have successfully engineered the viscosity with the addition of EC to be in the 'optimal range' for ink-jet printing, as shown in figure 1, i.e. 8–12 cP, we can infer that the addition of EC in NMP does not alter the surface tension significantly.

The surface energy relation between liquid, solid and gas interfaces can be expressed by Young's equation

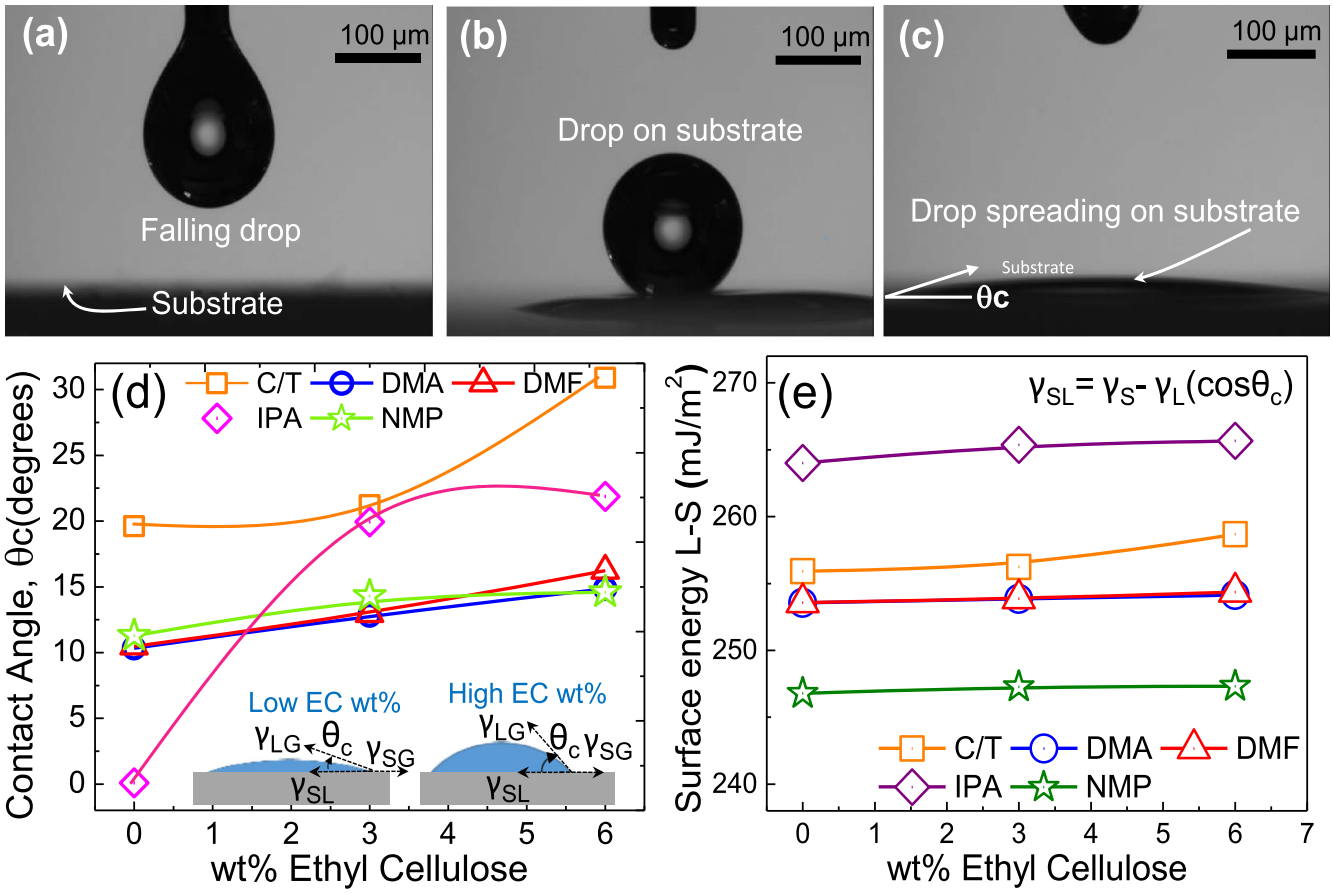

Figure 2. Illustration of contact angle measurement (C/T with 4 wt% EC) when: (a) drop falling, (b) drop as it touches substrate, (c) and as the drop settles on the surface. (d) Contact angle variation with EC addition. Inset showing a small and a high contact angle. (e) Interface energy change with addition of EC including Young's equation.

$\gamma_S = \gamma_{SL} + \gamma_L \cos\theta c$, where γ_L is the surface tension of the liquid, γ_{SL} is the surface energy between solid to liquid interface, and γ_S is the surface energy of the solid [28, 39, 40]. We have calculated the surface energy of the liquid—solid interface (γ_{SL}) from the measured θ_c of different solvents. For example, for IPA 3 wt% EC, θ_c was measured ~19°, and given the surface energy for $SiO_2 \sim 287\ mJm^{-2}$, from the Young's equation we obtained an interface surface energy value of $265\ mJm^{-2}$. It is important to note that for γ_L, we assumed the initial surface tension values for the respective solutions, i.e., γ_L values for IPA, C/T, DMA, DMF and NMP are $23\ mJm^{-2}$, $33\ mJm^{-2}$, $34\ mJm^{-2}$, $34\ mJm^{-2}$ and $41\ mJm^{-2}$, respectively. Figure 2(e) shows the variations in the liquid-solid surface energies with increasing EC concentration which indicate the interface surface energy between the liquid drop and the SiO_2 substrate was not modified by more than 5% with the addition of EC, which is likely due to the substantially larger substrate surface energy ~$287\ mJm^{-2}$ for SiO_2 (figure 2(e)).

2.2. MoS_2 dispersions and their stability

After the η and γ are optimized through the addition of EC, we proceeded to formulate dispersions of 2DLMs. Here we discuss the results related to the MoS_2 dispersion which was prepared using MoS_2 powder and adding 1 wt% EC for controlling dispersion viscosity. Two sonication times were investigated (0.5 h and 6 h) followed by a 24 h stabilization period. Optical absorbance spectroscopy was used to investigate the MoS_2 dispersion (figure 3(a)) which indicates the absorption increased as the sonication time increased, due to particle size and/or layer number reduction. This is also visualized by the physical appearance of the vials in the inset of figures 3(b)–(f), where the solution appears darker with the greater sonication time for the solvents investigated. The C/T absorbance was greatest, followed by DMF, NMP, DMA, and IPA. The characteristic peaks for MoS_2 at 608 nm and 665 nm [41, 42] were observed in C/T and NMP, and mildly in the other solvents, which is related to excitonic behavior in ultra-thin nanosheets, and we will report on this characteristic in greater detail in forthcoming work [43]. Our aim in conducting this study was to look at differences between 'low' sonication exposure (as noted by the 0.5 h samples) and 'high' exposure (as noted by the 6 h samples). We believe that the important fact elucidated from our analysis here is that the relative absorbance generally seems to increase over the entire spectral range considered (350 nm–800 nm) for all the solvents at the high exposure level, as illustrated by the data in figures 3(a)–(f) for MoS_2. Hence, we infer that the dispersability and exfoliation of MoS_2 increases for the 6 h

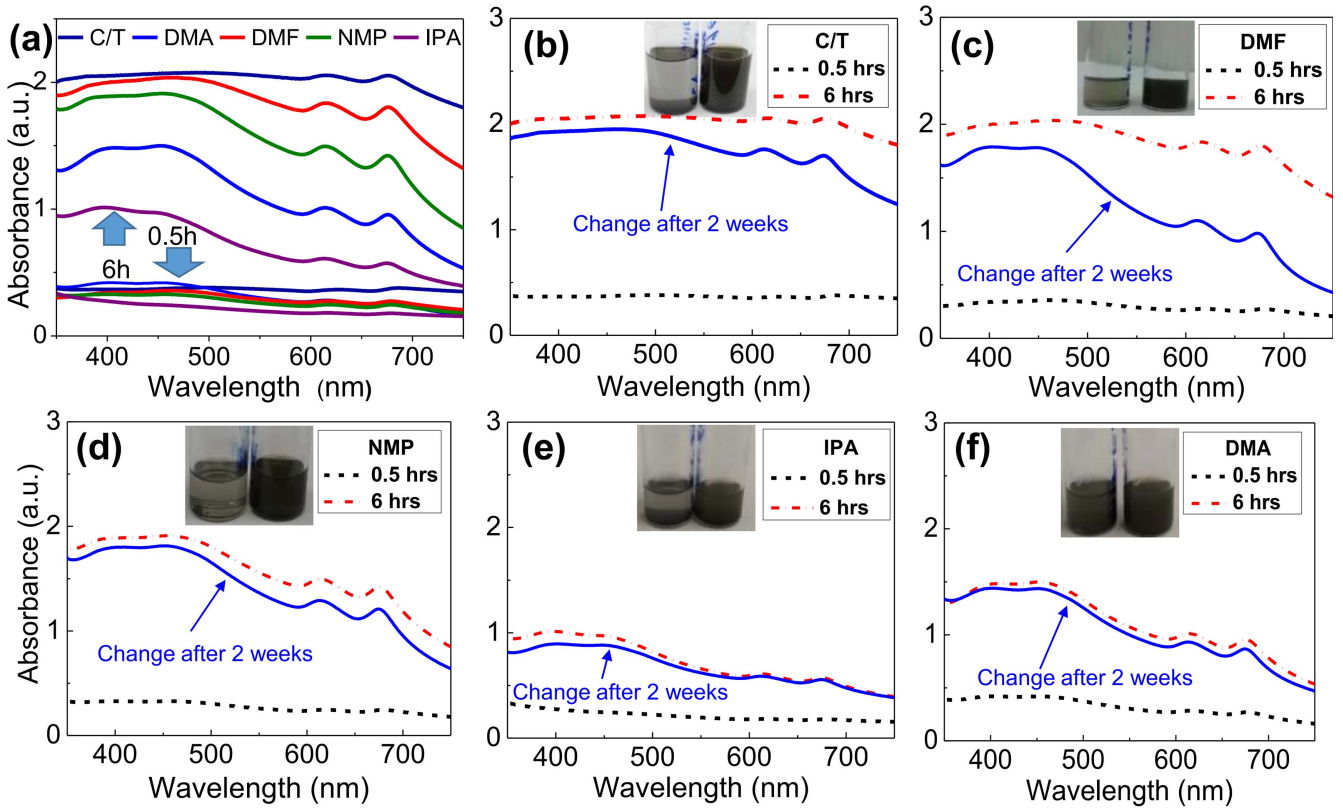

Figure 3. (a) Absorbance spectra of MoS_2 dispersions after being sonicated for 0.5 h and 6 h as indicated by arrows. Absorbance for MoS_2 in (b) C/T, (c) DMF, (d) IPA, (e) NMP and (f) DMA, showing optical spectra after 0.5 h and 6 h of sonication, and after two weeks of storage. Inset shows the visual images of the dispersions for 0.5 h and 6 h in all solvents, demonstrating the difference in nanoparticle concentration.

sonication or higher exposure condition, compared to the lower exposure condition of 0.5 h.

The stability of the dispersions over time was also explored for the 6 h sonicated samples, which indicated a high degree of suspension stability for DMA followed by IPA, NMP, C/T, DMF (see figures 3(b)–(f)). In the case of DMF, a pronounced decrease in the absorbance after a two-week 'settling' period was observed, possibly due to particulate re-agglomeration. We are in the process of exploring the electronic properties of the MoS_2 dispersions in more detail, and now turn to our analysis and characterization of the graphite dispersions, as described in sections 2.3–2.6.

2.3. Graphite dispersions

Two sources of graphite were used as the starting templates for generating the graphite/graphene dispersions, namely commercially available graphite rod (GR), which is an untreated or 'natural' graphite, as well as graphite powder (GP) which is an artificially compressed graphite powder (GP). In the first case, the GR was broken into pieces and sonicated in each of the five solvents. Figure 4(a) depicts a scanning electron micrograph (SEM) of the broken GR pieces, as purchased from the manufacturer (inset), with its layered structure (see arrow in figure 4(a)). The GR flake distribution varied from a few microns to almost 50 μm. In the second case of the GP, the SEM micrograph in figure 4(b) reveals large particles (see black arrow) with particle distribution ranging from 100 μm to 700 μm, ~10X larger than the flake size distribution in the GR. Therefore in the GR case, the layered structure can be clearly visualized through the platelet-like lamellar structure observed (figure 4(a)), while the GP is composed of a carbon where this platelet-like structure is non-evident, and the material resembles solid, 'dense pebbles' (figure 4(b)). Given the highly compressed nature of the GP in figure 4(b), the higher density and absence of interlayers is likely to inhibit the penetration of the solvent to effectively exfoliate the material using solution-based processing.

The GR was successfully dispersed in all five solvents by sonicating for 6 h, as shown by the vials in the inset of figure 4(c), including water. Despite its benign nature, even the water-based graphite dispersion showed discoloration indicating the exfoliation of graphite flakes occurring, to some extent, in water [43]. We plan to conduct a more detailed analysis for developing efficient water-based 2D dispersions which may open up prospects for utilizing such dispersions for more eco-friendly applications in the future. The SEM micrograph of the drop-cast GR dispersion in NMP (on SiO_2/Si) is shown in figure 4(c), which resulted in small pinholes in the film, but in contrast, a very sparse distribution of randomly distributed particles in the GP film was observed, as shown in figure 4(d). Thus, the GR flakes seem to form a continuous film (figure 4(c)), which was not observed for the GP.

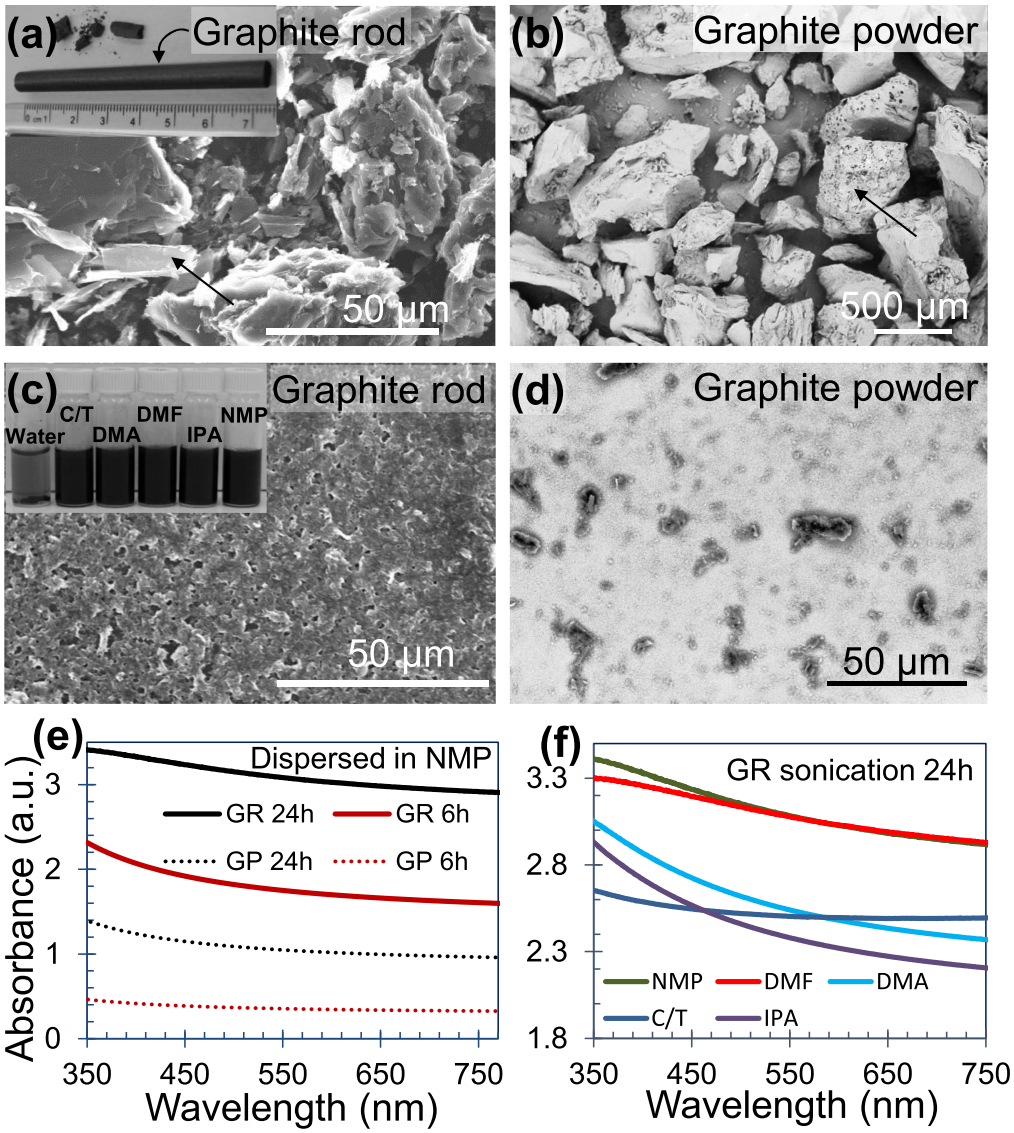

Figure 4. (a) SEM micrograph of graphite rod powder, with inset showing graphite rod as obtained from the manufacturer. (b) SEM micrograph of graphite powder (c) SEM micrograph of GR ink applied on SiO_2, with inset showing GR dispersions in all five solvents and water. (d) SEM micrograph of GP dispersion drop cast on SiO_2. (e) Absorbance comparison between graphite rod and graphite powder for 6 and 24 h. (f) Absorbance of GR in five solvents sonicated for 24 h.

Optical absorption spectroscopy for the GR and GP suspensions (without EC) in NMP are shown in figure 4(e), for sonication times of 6 h and 24 h. The GR suspension exhibits higher absorbance, and hence a higher concentration dispersion, at both sonication times compared to even the 24 h sonication of the GP. We believe that the layered structure of the graphite rod results in a higher concentration of nano-dispersed particles in solution, and consequently a continuous film morphology results after the drop-casting process. This result comprehensively demonstrates that the GR is a useful starting template for formulating inks for ink-jet printing, given its layered structure in contrast to the GP. For this reason we have chosen GR as the raw starting material for formulating our dispersions for ink-jet printing, which we report on from hereon. Figure 4(f) shows the variation in the optical absorbance spectra for the GR, which indicates that the NMP and DMF yielded a higher optical absorbance in comparison to all of the other solvents, a signature of the higher dispersion density in this case.

2.4. Role of Ethyl Cellulose

Ethyl Cellulose has been used in the coatings industry for several decades and is long known to be a rheology modifier [44]. Here we explore its role in the ink formulation process of our 2DLMs. In prior work, EC has been used as a dispersant surfactant for inkjet printing of 2DLMs [24, 31], where it is usually added to the solution mixture before sonication in order to promote EC intercalation deep into the graphite layers to prevent particle aggregation [27, 45, 46]; however, this process reduces the effective sonication power density experienced by individual particles, and consequently reduces flake exfoliation. In our study we have demonstrated that adding EC to the GR before sonication resulted in much

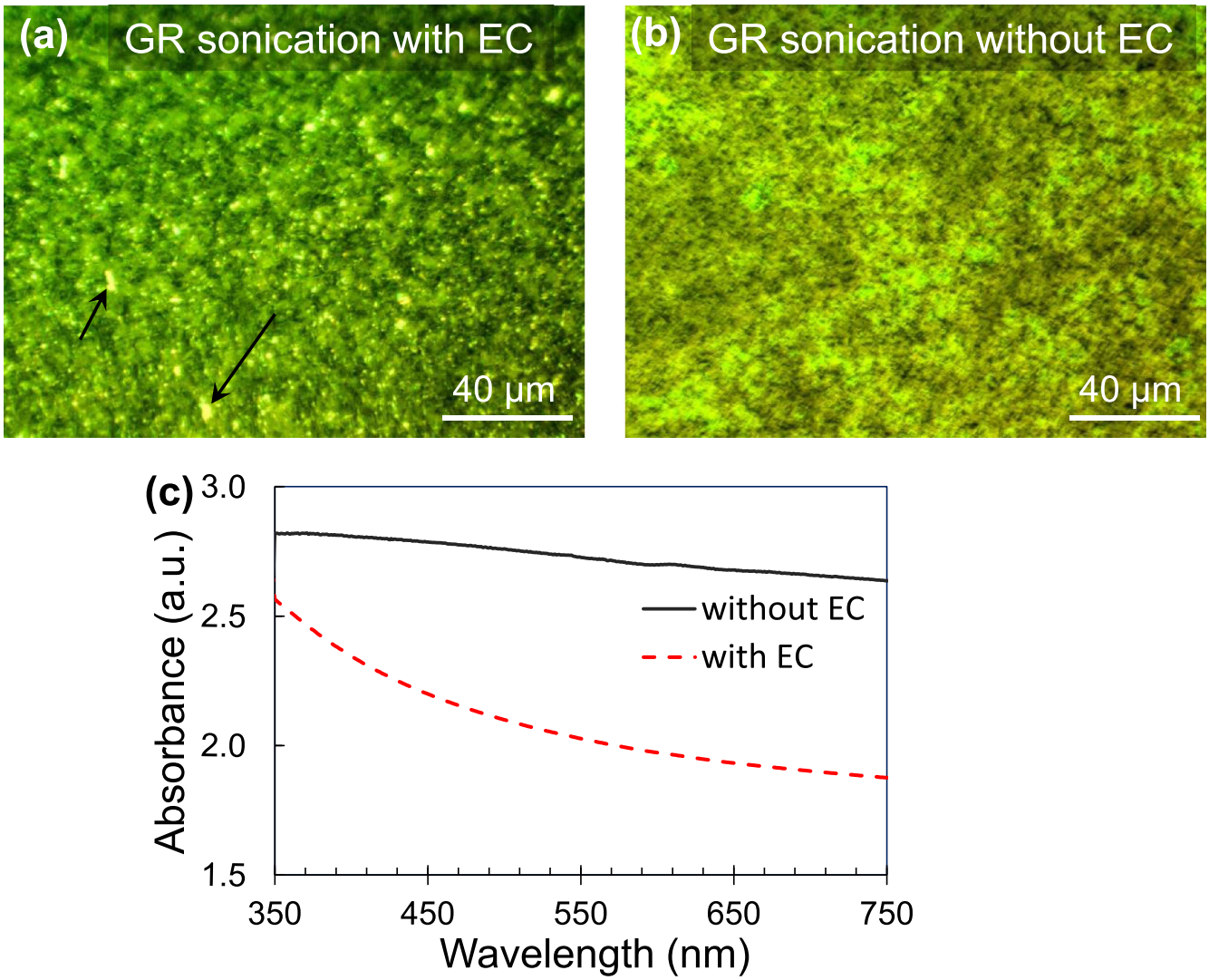

Figure 5. (a) Optical image of GR dispersed in NMP and sonicated for 24 h **with** EC added (b) Optical image of GR dispersed in NMP and sonicated for 24 h **without** 4% EC added. (c) Comparison of absorbance for GR dispersed in NMP sonicated 24 h with and without EC.

larger particle size, as shown by the black arrow in figure 5(a) of the optical micrograph image of the drop-cast surface, which is likely due to the reduction of the effective sonication power density. This is in contrast to the image in figure 5(b) (without EC) where no large particles are detected at the same magnification. The optical spectra in figure 5(c) also corroborates the higher density dispersion for the case without the EC, given the higher optical absorbance in this case. This suggests the EC acts as a 'shock absorber' in the sonication process and reduces the effectiveness of the exfoliation. The addition of EC has the purpose of preventing particle aggregation, a phenomenon that will occur primarily after the sonication has been completed. In our work, we conclude that EC should be added after sonication, since its addition before sonication will likely diminish the overall intensity of the ultrasonic waves, and reduces the effective exfoliation of the materials. While sonication is proceeding, there is little chance for particles to re-aggregate, and hence EC can be added after sonication to prevent nanoparticle aggregation.

2.5. Electronic properties and morphology characterization of 2D-graphite dispersions

GR dispersions were drop-cast onto SiO_2 substrates and annealed at 350 °C for 60 min and their electronic transport properties measured. Illustrated in figure 6(a) is an I-V characteristic of the GR dispersion in all five solvents, while the inset depicts the GR film resistance. Using two-terminal measurements, the GR dispersion in DMF exhibited the lowest resistance (1.6 KΩ) compared to C/T which yielded the highest resistance (18 KΩ) for the same electrode spacing and approximate thickness. The image in figure 6(b) is indicative of a uniform film morphology for the DMF sample, unlike the NMP sample shown in figure 6(c), which exhibited a rougher and more non-uniform film morphology (see yellow arrows). From our initial observations, we have found that the drop-cast samples from the C/T dispersion appeared to form a non-uniform film. The non-uniform film morphology is likely the reason for the high resistance observed in this case. While the GR dispersed in DMF exhibits the lowest resistance in drop-cast films compared to other solvents, it

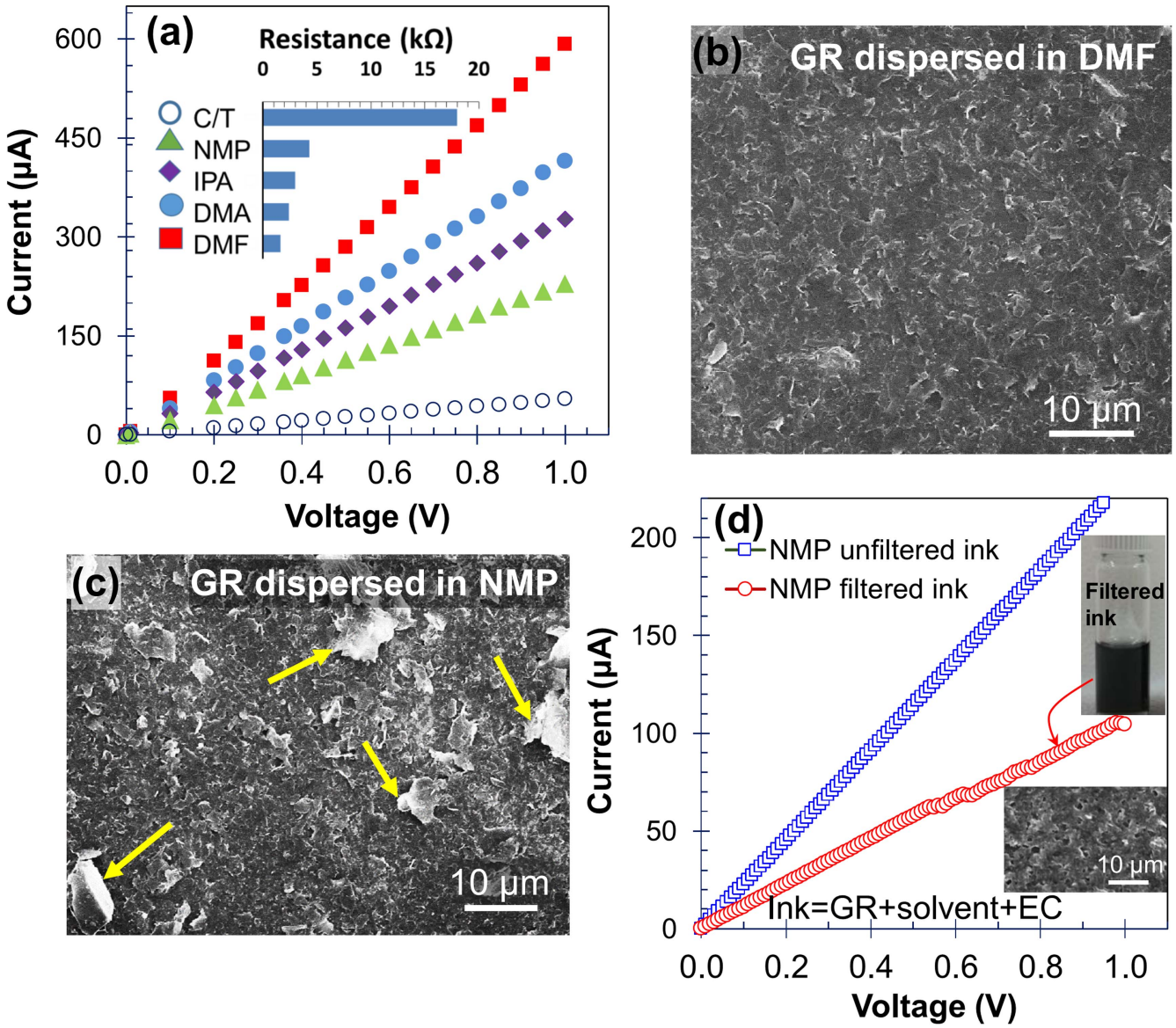

Figure 6. (a) I-V curves of GR dispersed in five solvents after being drop cast on SiO_2 wafer and annealed for 1 h at 350 °C. (b) SEM micrograph film resulting from dispersion of GR in DMF. (c) SEM micrograph film resulting from dispersion of GR in NMP. (d) I-V curves of NMP unfiltered and filtered ink after being drop cast on SiO_2 wafer and annealed for 1 h at 350 °C (inset shows SEM image and dispersion vial).

requires the addition of ~6 wt% of EC compared to ~4 wt% required for NMP to yield optimum viscosity and printability (10 cP) (see figure 1). For this reason, the dispersion of GR in NMP was used in the ink preparation for printing given its higher particle dispersion as deciphered from optical absorption spectroscopy data (shown in figure 4(d)).

Since a particle size below 200 nm is necessary to avoid nozzle clogging in our ink-jet printer, the dispersion (GR + NMP solvent + EC) was filtered using a 0.2 μm syringe filter. Electronic transport measurements were conducted for the unfiltered and filtered inks as shown by the I-V characteristic in figure 6(b). Resistance values obtained for the filtered and unfiltered ink were 9.6 kΩ and 4.3 kΩ, respectively. While the filtered ink exhibited a higher resistance, this is not surprising due to the removal of more graphite precipitates during the filtration process. The top inset in figure 6(b) shows the relatively dark black color of the filtered ink in the vial, which is suggestive of a high concentration nanoparticle dispersion, while the bottom inset shows the relatively smooth surface morphology of the drop-cast ink onto SiO_2 that explains its reasonable electronic transport characteristics.

2.6. Ink-jet printing of 2D-graphite dispersions

Ink-jet printing of our 2D graphite ink was performed using a DIMATIX 2831 ink jet printer, which utilizes the micro-electro-mechanical (MEM)-based piezoelectric actuation mechanism. The NMP ink was successfully printed onto SiO_2/Si substrates, as shown in figure 7(a) which represents an array of ink-jet printed lines of graphite formulated NMP-based inks. Figure 7(b) shows the high-magnification optical

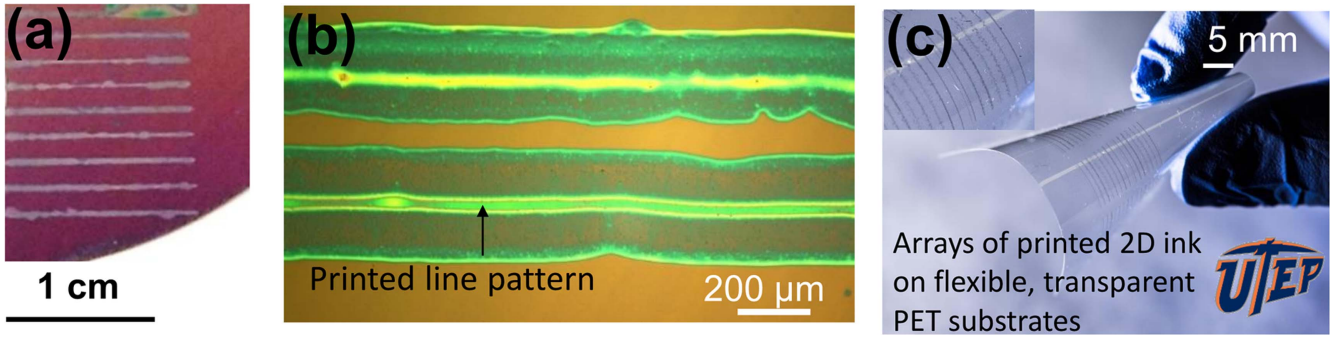

Figure 7. (a) Digital image showing printed lines patterned with the prepared ink on SiO_2 substrate. (b) Optical image of SiO_2 substrate with printed pattern. (c) Digital image of a printed line pattern on flexible, transparent PET substrate over large areas; top left inset depicts a magnified region of the printed lines on PET.

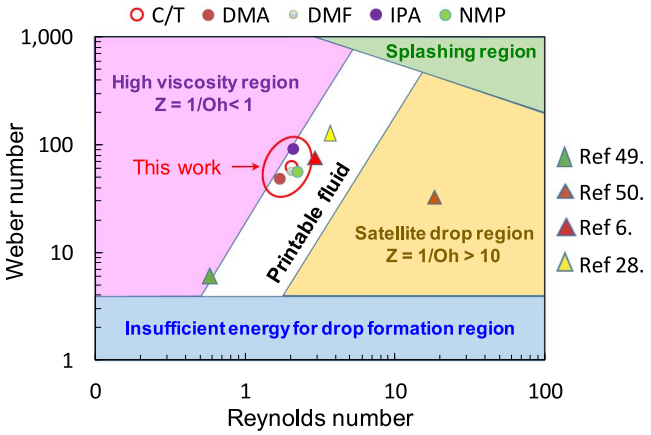

Figure 8. Ink fluidic property plot, illustrating the effect of the Reynolds number and the Weber's number on the ink fluidic properties. This indicates different regions for fluid mechanics, and the optimal region for stable drop formation and jettability. Mapped onto this plot is work from [6, 28, 49], and [50] for comparative analysis.

micrograph of two printed lines on the SiO_2 substrate with a line-width of ~240 μm. This image illustrates the ink solution is concentrated in the center of the line due to the well-known Marangoni effect [27, 47, 48], in which nano-dispersed ink particles tend to move towards the higher concentrated regions. Figure 7(c) illustrates the promise of our ink-jet printed graphite ink that was successfully printed onto a flexible and transparent substrate, specifically polyethylene terephthalate (PET).

As stated earlier, the ink fluidic properties are represented by the Reynolds ($\mathrm{Re} = \upsilon\rho a/\eta$), Weber ($\mathrm{We} = (v\hat{}2\ \rho a)/\gamma$), Ohnesorge ($\mathrm{Oh} = (\sqrt{\mathrm{We}})/\mathrm{Re}$), and $Z = 1/\mathrm{Oh}$ numbers, where v is the drop velocity. The ink fluidic property can be represented in a plot of *Re* versus *We* [23, 27, 46, 47], (see figure 8) which illustrates the impact of γ ρ, η on the ink-jetting characteristics. The fluid position on the map can be modified as indicated by the arrows with an increase in the v, ρ, η, or γ. Furthermore, this plot can define optimum printing regions by specifying inadequate drop dynamics regions, such as viscous, splashing, satellite drop, and insufficient energy for drop formation, as shown in figure 8. Through our experiments, we clearly see that our inks are well within the printable fluid region (see red dashed oval in figure 8) for optimum printing for the synthesized dispersion of GR in NMP. The combination of η and γ for our dispersions has resulted in printable inks with *Re* from 1.7 to 2.2 and *We* of 48 to 90, close to the limit of printable fluids. Results from previous investigations have also been mapped onto this plot for comparison [49, 50]. For example, in [6] and [28], the inks were clearly inside the 'printable' region, while others are further from the boundaries (references [49] and [50]). It should be noted that the ink position on the fluidic property plot can also be modified by changing printer parameters, such as firing voltage, jetting waveform, standing time, cartridge and substrate temperature, to some extent, which can provide another degree of freedom for potentially targeting the ink properties toward the printable fluid regime.

3. Conclusions

We have obtained high-quality inks using C/T and NMP as solvents for MoS_2 and graphite dispersion, respectively. NMP resulted in high GR nano-flake dispersion, low resistive printed pattern, and good printability. The addition of EC as a surfactant not only prevents the agglomeration of nano-particles, but can be an important avenue for engineering the η of a solvent to make it suitable for ink-jet printing. The effect of EC in modifying θ_c of a solvent seems to be related to P_i of the solvent, with lower P_i (IPA and C/T) showing greater increase in θ_c for a given addition of EC. While EC has been added to the solution as surfactant before sonication in prior reports, we believe this reduces effective sonication power density to the individual particle clusters and reduces flake exfoliation efficacy. In our study we have noted that EC should be added to the solution mixture after sonication to prevent particle agglomeration, improve suspension stability, and achieve optimum solution viscosity for printing. We have observed GR with its layered structure results in higher nano-dispersed particle concentration in the aqueous suspension compared to GP. Furthermore, GR results in a more continuous film morphology, and low resistance after printing. We believe this comprehensive study of MoS_2 and graphite dispersions in the five different polar solvents, changing ink viscosity by controlling EC amount, addition of EC to the

solution mixture (before or after sonication), and the use of GR with its layered structure in formulating the inks, will be highly valuable for developing electronic and opto-electronic devices and sensors for printed electronics applications using 2DLM-based inks.

4. Experimental section

4.1. Viscosity study

The five solvents used in this work were purchased from Sigma Aldrich and used as received, with the exception of the C/T mixture which was prepared at a ratio of 7:3 throughout the experiments. EC was obtained from Sigma Aldrich 200646. Contact angle measurements were performed using a Ramehart 250 F4 standard goniometer. MoS_2 was commercially obtained (Sigma Aldrich #69860), and in all the dispersions it was prepared with an initial concentration of 3 mg ml^{-1}, as was the dispersion for the Graphite Rod (Sigma Aldrich #496553) and graphite powder (Alfa Aesar #10131). *Characterization:* optical absorption spectroscopy was conducted using a CARY 5000 spectrophotometer in quartz cuvettes with 0.3 ml volumetric capacity. SEM microscopy was carried out in a Hitachi S-4800. Whenever dispersion samples were drop cast on wafers, SiO_2 wafers with a 300 nm oxide layer were used. Electrical characterization was conducted using a micromanipulator 450PM-B probe stage equipped with a HP precision semiconductor parameter analyzer 4156A. *Printing*. The DIMATIX 2831 material printer from Fujifilm was used for the ink jet printing, where the ink cartridges were purchased from the manufacturer and had a volume of 10 pl and equipped with 200 nm syringe filters. The cartridges were comprised of 16 nozzles, where the nozzle diameter was ~21.5 μm.

Acknowledgments

We would like to thank Mr Alberto Delgado for his assistance in taking some of the SEM images. A B K acknowledges the University of Texas System Faculty Science and Technology Acquisition and Retention (STARS) award (EC284802) for the acquisition of equipment in the establishment of the Nanomaterials and Devices Lab at the University of Texas, El Paso (UTEP). Support provided by the UTEP start up grant is also acknowledged for MM. We also thank the Air Force Office of Scientific Research (grant number FA9550-15-1-0200) that enabled us to pursue this work.

References

[1] Novoselov K, Geim A, Morozov S, Jiang D, Zhang Y, Dubonos S, Grigorieva I and Firsov A 2004 Electric field effect in atomically thin carbon films *Science* **306** 666–9

[2] Novoselov K, Booth T J, Khotkevich V V, Morozov S V, Geim A K and Rice T M 2005 Two-dimensional atomic crystal *Proc. of the Natl Academy of Sciences USA* **102** 10451

[3] Mingsheng X, Liang T, Shi M and Chen H 2013 Graphene-like two-dimensional materials *Chemical Reviews* **113** 3766–98

[4] Song L, Ci L, Lu H, Sorokin P B, Jin C, Ni J, Kvashnin A G, Kvashnin D G, Lou J and Yakobson B I 2010 Large scale growth and characterization of atomic hexagonal boron nitride layers *Nano Lett.* **10** 3209

[5] Wilson J and Yoffe A 1969 The transition metal dichalcogenides discussion and interpretation of the observed optical, electrical and structural properties *Advanced Physics* **18** 193–335

[6] Coleman C, Goldwhite H and Tikkanen W 1998 A review of intercalation in heavy metal iodides *Chem. Mater.* **10** 2794–800

[7] Song L, Liu Z, Reddy A L M, Narayanan N T, Taha-Tijerina J, Peng J, Gao G, Lou J, Vajtai R and Ajayan P M 2012 Binary and ternary atomic layers built from carbon, boron, and nitrogen *Adv. Mater.* **24** 4878–95

[8] Nicolosi V, Chhowalla M, Kanatzidis M G and Strano M S 2013 Liquid exfoliation of layered materials *Mater. Sci.* **340** 1226419

[9] Secor E B, Prabhumirashi P L, Puntambekar K, Geier M L and Hersam M C 2013 Inkjet printing of high conductivity, flexible graphene patterns *The Journal of Physical Chemistry Letters* **4** 1347–51

[10] Cai L and Wang C 2015 Carbon nanotube flexible and stretchable electronics *Nanoscale Res. Lett.* **10** 1–21

[11] Makarov D, Karnaushenko D and Schmidt O G 2013 Printable magnetoelectronics *ChemPhysChem* **14** 1771–6

[12] Muccini M 2006 A bright future for organic field-effect transistors *Nat. Mater.* **5** 605–13

[13] Singh M, Haverinen H M, Dhagat P and Jabbour G E 2010 Inkjet printing process and applications *Adv. Mater.* **22** 673–85

[14] Viculis L, Mack J and Kaner R 2003 A chemical route to carbon nanoscrolls *Science* **299** 1361

[15] Chen G, Weng W, Wu D, Wu C, Lu J, Wang P and Chen X 2004 Preparation and characterization of graphite nanosheets from ultrasonic powdering technique *Carbon* **42** 753–9

[16] Jana M, Saha S, Khanra P, Samanta P, Koo H, Murmu N C and Kuila T 2015 Non-covalent functionalization of reduced graphene oxide using sulfanilic acid azocromotrop and its application as supercapacitor electrode material *J. Mater. Chem.* **3** 7323–31

[17] Dreyer D R, Park S, Bielawski C W and Ruoff R S 2010 The chemistry of graphene oxide *Chem. Soc. Rev.* **39** 228–40

[18] Hernandez Y, Nicolosi V, Lotya M, Blighe F M, Sun Z, De S, McGovern I, Holland B, Byrne M and Gun'Ko Y K 2008 High-yield production of graphene by liquid-phase exfoliation of graphite *Nat. Nanotechnol.* **3** 563–8

[19] Kamat P V 2012 Manipulation of charge transfer across semiconductor interface. A criterion that cannot be ignored in photocatalyst design *The Journal of Physical Chemistry Letters* **3** 663–72

[20] May P, Khan U, O'Neill A and Coleman J N 2012 Approaching the theoretical limit for reinforcing polymers with graphene *J. Mater. Chem.* **22** 1278–82

[21] Lotya M, Hernandez Y, King P J, Smith R J and Nicolosi V 2009 Liquid phase production of graphene by exfoliation of graphite in surfactant/water solutions *Journal American Chemistry Society* **131** 3611–20

[22] Hasan T, V Scardaci V, Tan P, Rozhin A G, Milne W I and Ferrari A C 2007 Debundling' of singlewall carbon nanotube dispersions in N-Methyl-2-pyrrolidone (NMP) by polyvinylpyrrolidone *The Journal of Physical Chemistry* C **111** 12594–602

[23] Derby B 2010 Inkjet printing of functional and structural materials: fluid property requirements, feature stability, and resolution *Annu. Rev. Mater. Res.* **40** 395–414

[24] Coleman J, Lotya M, O'Neill A, Bergin S, King P, Khan U, Young K, Gaucher A, De S and Smith R 2011 Two-dimensional nanosheets produced by liquid exfoliation of layered *Mater. Sci.* **568** 331
[25] Derby B and Reis N 2003 Inkjet printing of highly loaded particulate suspensions *MRS Bull.* **28** 815–8
[26] Liang Y T and Hersam M C 2010 Highly concentrated graphene solutions via polymer enhanced solvent exfoliation and iterative solvent exchange *J. Am. Chem. Soc.* **132** 17661–3
[27] Li J, Lemme M C and Östling M 2014 Inkjet printing of 2D layered materials *ChemPhysChem* **15** 3427
[28] Torrisi F, Hasan T, Wu W, Sun Z, Lombardo A, Kulmala T S, Hsieh G W, Jung S, Bonaccorso F and Paul P J 2012 Inkjet-printed graphene electronics *ACS Nano* **6** 2992–3006
[29] Huang L, Huang Y, Liang J, Wan X and Chen Y 2011 Graphene-based conducting inks for direct inkjet printing of flexible conductive patterns and their applications in electric circuits and chemical sensors *Nano Res.* **4** 675–84
[30] Meyer J C, Geim A K, Katsnelson M, Novoselov K, Booth T and Roth S 2007 The structure of suspended graphene sheets *Nature* **446** 60–3
[31] Capasso A, Castillo A D R, Sun H, Ansaldo A, Pellegrini V and Bonaccorso F 2015 Ink-jet printing of graphene for flexible electronics: an environmentally-friendly approach *Solid State Commun.* **224** 53
[32] Joong T H, Jeong I J, Haena K, Jun Y H, Hyung K Y and Jong S W 2014 Extremely efficient liquid exfoliation and dispersion of layered materials by unusual acoustic cavitation *Sci. Rep.* **4** 1–7
[33] Ibrahem M A, Lan T W, Huang J K, Chen Y Y, Wei K H, Li L J and Chu C W 2013 High quantity and quality few-layers transition metal disulfide nanosheets from wet-milling exfoliation *RSC Advances* **3** 13193–202
[34] Kordás K, Mustonen T, Tóth G, Jantunen H, Lajunen M, Soldano C, Talapatra S, Kar S, Vajtai R and Ajayan P M 2006 Inkjet printing of electrically conductive patterns of carbon nanotubes *Small* **2** 1021–5
[35] Sungjin P, Jinho A, Inhwa J, Piner R D and Sung J A 2009 Colloidal suspensions of highly reduced graphene *Nano Lett.* **9** 1593–7
[36] Paredes J, Villar-Rodil S, Martinez-Alonso A and Tascon J 2008 Graphene oxide dispersions in organic solvents *Langmuir* **24** 10560–4
[37] De Gennes P G 1985 Wetting: statics and dynamics *Rev. Mod. Phys.* **57** 827
[38] Park J S, Kim, Song C and Lee M 2010 Control of inkjet printed profiles by solvent-vapor annealing *Displays* **31** 164–7
[39] Reis N and Derby B 2000 Ink jet deposition of ceramic suspensions: modeling and experiments of droplet formation *MRS Proceedings* **65** 65–70
[40] Anyfantakis M and Baigl D 2015 Manipulating the coffee-ring effect: interactions at work *ChemPhysChem* **16** 2726–34
[41] Wang J, Chen L, Lu W, Zeng M, Tan L, Ren F, Jiang C and Fu L 2015 Direct growth of molybdenum disulfide on arbitrary insulating surfaces by chemical vapor deposition *RSC Advances* **5** 4364–7
[42] Castellanos-Gomez A, Quereda J, van der Meulen H P, Agraït N and Rubio-Bollinger G 2016 Spatially resolved optical absorption spectroscopy of single-and few-layer MoS_2 by hyperspectral imaging *Nanotechnology* **27** 115705
[43] Fadil D, Fayaz H R, Lara G and Kaul A B 2016 Electrical transport and hot–luminescence effects in exfoliated MoS_2 and WS_2 2D-materials submitted
[44] Davidovich-Pinhas M, Barbut S and Marangoni A 2014 Physical structure and thermal behavior of Ethyl Cellulose *Cellulose* **21** 3243–55
[45] Stankovich S, Dikin D A, Piner R D, Kohlhaas K A, Kleinhammes A, Jia Y, Wu Y, Nguyen S T and Ruoff R S 2007 Synthesis of graphene-based nanosheets via chemical reduction of exfoliated graphite oxide *Carbon* **45** 1558–65
[46] Niyogi S, Bekyarova E, Itkis M E, McWilliams J L, Hamon M A and Haddon R C 2006 Solution properties of graphite and graphene *J. Am. Chem. Soc.* **128** 7720–1
[47] Shih C J, Lin S, Strano M S and Blankschtein D 2010 Understanding the stabilization of liquid-phase-exfoliated graphene in polar solvents: molecular dynamics simulations and kinetic theory of colloid aggregation *J. Am. Chem. Soc.* **132** 14638–48
[48] Sun J, Bao B, He M, Zhou H and Song Y 2015 Recent advances in controlling the depositing morphologies of inkjet droplets *ACS Applied Materials & Interfaces* **7** 28086–99
[49] Jang D, Kim D and Moon J 2009 Influence of fluid physical properties on ink-jet printability *Langmuir* **25** 2629–35
[50] Yu-Feng L, Ming-Hsu T and Yen-Fang P 2013 Control of droplet formation by operating waveform for inks with various viscosities in piezoelectric inkjet printing *Appl. Phys.* A **111** 509–16